STATE RESEARCH CENTER OF RUSSIA
INSTITUTE FOR HIGH ENERGY PHYSICS
RU-142284, Protvino, Moscow Region, Russia

NuMI–B–675
August 10, 2000

Dynamic Stress Calculations for ME and LE Targets and Results of Prototyping for the LE Target

(Task B Report of the Accord between FNAL and IHEP)

A.Abramov, S.Filippov, N.Galyaev, V.Garkusha,
R.Gibadullin*, I.Ponimash*, A.Ryabov, V.Zarucheisky

*) Institute of Physics and Power Engineering, Obninsk, Kaluga region, Russia

Contents

1 Introduction

This Report is an extension of target designs for the NuMI Medium Energy (ME) and Low Energy (LE) beams [1]. Because of the large average power deposited in a target by the 120 GeV and 4×10^{13} protons per spill primary beam, the fin shape of a target with its conducting cooling and subsequent transferring of a heat to the water cooling system was chosen as the base conception for both target designs. Graphite ZXF-5Q of Poco Graphite, Inc. and beryllium S-65C of Brush Wellman, Inc. were considered as possible target materials.

After completion of target prototype beam tests, the final package of drawings for the ME target was produced under the terms of the 1999 Accord between FNAL and IHEP. The advanced conceptual design of the LE target is given in the Task E report of that Accord [2]. **Section 2** of this Report gives a brief description of both target designs and summarizes results of temperature and stress calculations.

Taking into account a possible use for NuMI beams of the single turn extracted primary proton beam, **Section 3** gives results of calculations of dynamic stresses which arise in the ME and LE targets and in the beam plug due to very short heat load of a target material by a primary beam. As it is shown, the stress waves created at these conditions will not destroy the target material, although somewhat decrease the "safety factor" for graphite targets.

Preceding production of the final package of drawings, prototyping of main units of the LE target were produced in order to test the general construction technique and to test that alignment tolerances can be met. **Section 4** describes results of prototyping which cover the problems of connection (welding or soldering) of different materials used in the LE target design. Manufacturing of the 20-segments prototype of target core has verified the reality of the full scale LE target construction within required tolerances.

2 General Description of NuMI Target Designs

The choice of the target material and sizes has been based on an optimization taking into account factors of the neutrino event rate and the reliability of a target operation during at least 10^7 pulses per one year [1]. Because of the large average power (1.6–2.4 kW) deposited in a target by the 120 GeV and 4×10^{13} protons per spill primary beam, the fin shape of a target with its conducting cooling and subsequent transferring of a heat to the water cooling system was chosen as the base conception of a target design for all WBB configurations of the PH2 focusing system. The elliptical shape of a primary beam spot with relationships $\sigma_y \simeq 2\sigma_x$ and $d \simeq 4.5\sigma_x$ between primary beam spot sizes and the thickness (width) of a target were found as close to optimal ones during a target design. Graphite ZXF-5Q of Poco Graphite, Inc. and beryllium S-65C of Brush Wellman, Inc. were considered as possible target materials.

Following from the focal length (the depth of field) of the focusing system and from maximum production angles of secondaries accepted by the focusing system, there are no fundamental differences in the target design for ME and HE beams, which could differ only by the total length of a target and the average density of a target material.

To maximize the neutrino event rate, a target for the LE beam is placed on 2/3 of its length inside the first horn; therefore the maximum transverse size of a target design is limited by the internal diameter of the horn inner conductor (~40 mm) at the downstream end of a target.

In both considered target designs the elements of a cooling system and target casing should be located beyond reach the mis-steered primary proton beam. Its possible trajectories in the focusing system are restricted in transverse directions with help of the baffle protection collimators, which prevent direct hitting of horn necks by the mis-steered primary beam.

2.1 ME Target Design

The general view of the ME target design is shown in Figure 2.1. The primary proton beam travels through the top of twelve 3.2 (4.1) mm thick and 100 mm length graphite (beryllium) plates, which are pressed with help of twelve pressing plates to the base plate having two channels for cooling water passing. Necessary pressure (~2 atm) is provided by two springs per one target plate. To prevent an absorption of secondaries contributing to the neutrino flux in the detector, the upper cooling channel is lowering continuously along the base plate. The base and pressing plates are made of an aluminum alloy and anodized with the 30 μm thick alumina in order to have charge-read-out (Budal) monitoring of an efficiency of a primary beam interaction with each target plate.

To decrease the quasi-static thermal stresses in a material, each graphite target plate is cut from its top into four 22 mm length and 30 mm height segments (teeth). In case of the beryllim target each plate consists of five 16.8 mm length segments. Segment corners are rounded with the radius equal to one half of the segment thickness, that allows to relieve significantly the stress concentration.

All parts are inserted into the 7 mm thick and 290 mm diameter aluminum casing with a length of ~1.5 m. Two flanges with 0.5 mm thick beryllium windows separate the internal volume from a surrounding environment, while a vacuum or helium atmosphere inside target casing prevents contact of a target material with an air. The diameter of the upstream window is equal to 45 mm. The diameter of the downstream window is determined by the maximal angle of secondaries accepted by the focusing system and should not be less than 120 mm.

To provide a good thermal contact between target plates and the base plate during the full intensity regular operation mode, the target casing will be filled by a helium atmosphere. At the stage of a target alignment in the beam-line the vacuum inside the target casing is preferable from the point of view of charge-read-out monitoring of a target.

2.2 LE Target Design

The LE target core constitutes the row of 3.2 (4.1) mm thick and 20 mm height graphite (beryllium) segments soldered to two stainless steel cooling pipes with the external diameter of 4.0 mm and the wall thickness of 0.2 mm (Figure 2.2) [2]. The graphite target core consists of 47 segments with the length of 20 mm, while in case of a beryllium target the core consists of 56 16.5 mm length segments. As in the ME target design, the corners of each segment are rounded with the radius equal to one half of the segment thickness. To avoid a contact of heated segments, they are separated by 0.3–0.4 mm gaps.

The target core is inserted into the 0.4 mm thick and 30 mm diameter aluminum casing and is fixed there with help of three aluminum spacers. Spacers are anodized with the 30 μm thick alumina to provide an insulation of the target core for charge-read-out monitoring of a target. Because the downstream end of the LE target is located closely (~5 mm) to the inner conductor of the first horn, metal-ceramic adapters are used to separate target casing and water cooling pipes from the ground and to prevent an electrical discharge from the first horn to the target. The target canister with a ConFlat flange, as well as target casing and two beryllium windows separate the internal volume, which is pumped out or filled with a helium to protect the target material from the oxidative action of an air.

The total length of the LE target unit is equal to ~1.2 m. There are two possible ways to mount this target inside the first horn. The first one is that the target has its own support module like the ME target and another one — to mount the target to the outer conductor of the first horn. The 0.6–0.8 mm sag of a target, which is fixed at its upstream end, may be not taken into account because it is significantly smaller than the vertical size of target segments and the size of beam in this direction.

2.3 Results of Temperature and Quasi-Static Stress Calculations

The energy deposition in a target material was calculated with help of the MARS [3], while the ANSYS was used for calculations of temperature and thermal stress distributions. Calculations of target temperatures were made under the following boundary conditions:

- the thermo-resistance between a target material and a base plate (cooling pipes for the LE target design) is equal to zero. The input temperature of a cooling water is equal to 20°C;
- the heat transfer coefficient to a water is equal to 10 kW/m$^2\cdot$K;
- the radiation with the coefficient of a blackness equal to 1.0 was taken into account in case of the ME target.

Operational temperatures of target segments with the highest energy deposition density are given in Table 2.1. Because of the higher efficiency of the LE target cooling system, which consists of two cooling lines located as close as possible to the primary beam axis, operational temperatures of

LE targets are smaller than those of ME targets. The steady-state reaches in 30–40 proton spills for the ME target and in 4–5 spills for the LE one.

Target material	Graphite		Beryllium	
Target design	ME	LE	ME	LE
Primary beam spot size $\sigma_x \times \sigma_y$, mm^2	0.7×1.4		1.0×2.0	
Energy deposition density D_e, GeV/cm^3	0.092		0.045	
Thickness of segment d, mm	3.2		4.1	
Segment length l, mm	22	20	16.8	16.5
Temperature after the beam spill T_{max}, °C	593	344	186	125
Temperature rise ΔT, °C	187	251	65	75
Temperature before the beam spill T_{min}, °C	406	93	121	50
Maximal equivalent stress S_{eq}, MPa	19.5	24.4	148	150

Table 2.1: Temperatures at the beam axis and quasi-static thermal stresses in target segments with the highest energy deposition density.

Results of calculations of quasi-static thermal stresses show, that for both ME and LE target designs:

- the target material is subjected to the all-axis compression in the center and is stretched at lateral sides of a target segment with the significant stress concentration at non-rounded segment corners;

- the maximal stresses arise in the horizontal (perpendicular to the fin direction) cross-section of a target segment by the beam axis plane and grow with increasing of a segment length.

For chosen segment lengths the maximal equivalent (Von Mises) stresses are given in Table 2.1. In all considered cases these equivalent stresses occur at rounded corners of segments, while equivalent stresses in segment centers are somewhat smaller.

The high-cycle fatigue data for the S-200F VHP (Vacuum Hot Pressing) beryllium grade show [4, 5], that its 10^7 cycles fatigue endurance limit in both longitudinal and transverse directions is equal to 261 MPa, which coincide with the specified yield strength ($S_{0.2}$). The chosen for NuMI targets S-65C VHP grade is more pure than the S-200F grade and has the best resistance to a crack initiation and crack propagation depth at large thermal stresses. Assuming that fatigue properties of the S-65C grade are similar to those of the S-200F one and that the fatigue endurance limit varies with a temperature as the yield strength, the 10^7 cycles fatigue endurance limit for ME and LE targets may be estimated as 227 MPa and 240 MPa respectively (according to their operational temperatures). In this case the safety factor of $\sim$1.6 (the ratio of the fatigue endurance limit to the maximal equivalent stress occurring in target segments) is in existence for both ME and LE beryllium targets.

Because the graphite is a brittle material, the yield strength is not specified for it and, contrary to the beryllium, the graphite has different compressive and tensile strength limits, which are equal to 210 MPa and 95 MPa respectively for the ZXF-5Q grade with apparent density of 1.81 g/cm^3. Strength characteristics of the ZXF-5Q graphite grade grow with a temperature [6], but this increase is essential at the operational temperature more than 1000°C and may be neglected below 600–700°C. Fatigue tests for the graphite show [7], that at the stress cycled between zero stress and a tensile value, the 10^7 cycles fatigue endurance limit, expressing in terms of the homologous stress (the ratio of an applied stress to the first cycle strength), is in the range of 0.5–0.6. It means that for most loaded points of graphite segments, equivalent stresses are factor 2.7 and 2.1 (for ME and LE targets respectively) smaller than the fatigue endurance limit corresponding to the one year operation period of NuMI targets.

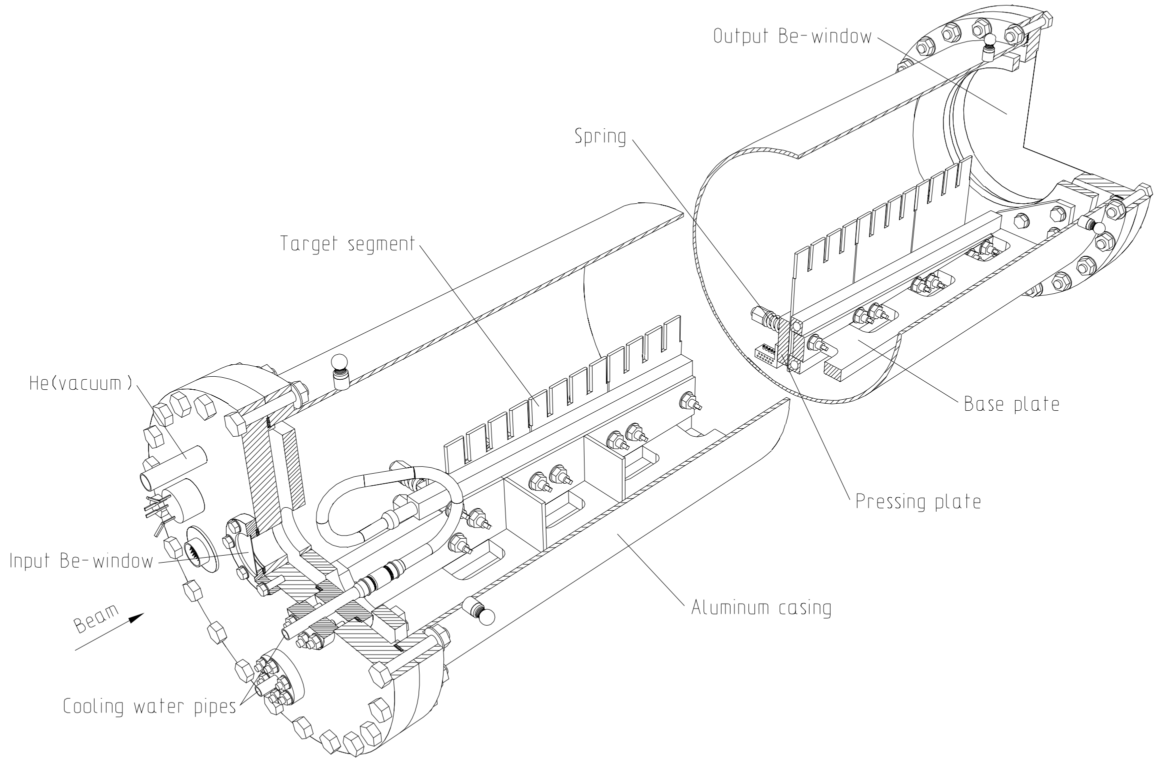

Figure 2.1: General view of the ME target design.

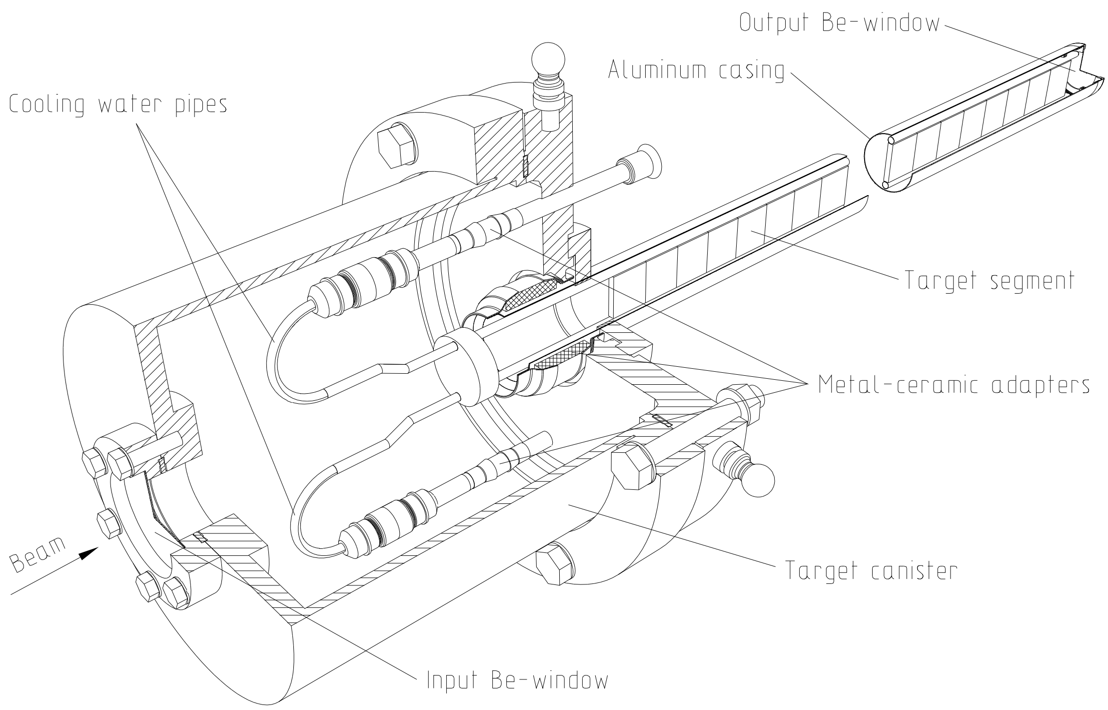

Figure 2.2: General view of the LE target design.

3 Dynamical Stresses in case of the Single Turn Extraction of a Primary Beam

The maximal dynamical stress, which arise due to very short heat load of a target material, is [8]

$$S_{max} \propto \begin{cases} \alpha E \Delta T & for \quad v_s\tau \leq l \\ \alpha E \Delta T (l/v_s\tau) & for \quad v_s\tau \geq l, \end{cases}$$

where α and E are the coefficient of thermal expansion and the modulus of elastisity respectively, ΔT is the adiabatic temperature rise, $v_s \simeq \sqrt{E/\rho}$ is the sound velocity, l is the length of a target segment and τ is the beam spill duration.

For the resonant extraction of a primary beam with $\tau \leq 1$ ms, the value of $v_s\tau$ is at least two orders of magnitude larger than the segment length l even for the graphite with the sound velocity of ~2.8 mm/μs (the sound velocity for the beryllium is equal to ~13 mm/μs), thus the analysis of stresses in targets may be restricted only by quasi-static stresses.

Otherwise, in case of the single turn extraction of a primary beam with $\tau = 8$ μs, $v_s\tau \simeq 22$ mm almost coincide with the length of graphite target segments. To check whether created at these conditions stress waves can not destroy the material, calculations of dynamic stresses were made with help of the ANSYS for LE and ME graphite targets[1] and for the beam plug.

The energy deposition density in the graphite was calculated assuming that distributions of a single turn extracted primary proton beam in the target are Gaussian in both transverse directions. As a result, for the proton beam with the $\sigma_x \times \sigma_y = 0.7 \times 1.4$ mm^2 spot size, the maximal energy deposition density on the beam axis increases up to 0.115 GeV/cm^3 in comparison with 0.092 GeV/cm^3 for the resonant extracted beam.

3.1 Dynamical Stresses in ME and LE Targets

The models of ME and LE targets used in dynamic stress calculations are shown in Figures 3.1 and 3.4. Similar to quasi-static thermal stresses in case of the resonant extracted primary beam, dynamical stresses were calculated in target segments with the highest energy deposition density.

[1]Taking into account results of stress calculations for the 100 mm length beryllium rod of the NGS beam target with $l/v_s\tau \simeq 0.8$ [9], one would expect that the lifetime of NuMI beryllium targets with $l/v_s\tau \simeq 0.16$ will be determined mainly by quasi-static thermal stresses.

Time evolution of stresses in various points of target segments are shown in Figures 3.2,3.3 for the ME target and in Figures 3.5,3.6 for the LE target. As it follows from given plots, the periods of stress components (and, correspondingly, of the equivalent stress) oscillations reflect dimensions of target segments, i.e. wave lengths of S_{xx}, S_{yy} and S_{zz} oscillations agree well with double thickness, height and length of segment respectively. Due to coupling of oscillations, the spectra of S_{yy} and S_{zz} stresses contains also the main frequency of S_{xx} oscillations. Coupling between oscillations of stresses in the beam axis plane of neighbouring target segments was not found in results of calculations.

The average and maximal equivalent stresses in two points of ME and LE target segments are given in Table 3.1. One should note, that the increase of equivalent stresses in different points of a target segment with respect to quasi-static thermal stresses in case of the resonant extraction (see Table 2.1) determines to a variable degree by a higher value of the maximal energy deposition density in the center of a target segment.

Despite of the fact, that in this case the equivalent stress reaches its maximal value in the center of a target segment, the point at the rounded corner continues to be a crucial point of a segment from the point of view of the material integrity, i.e. because of the all-axis extension of a target material the equivalent stress in this point should be compared with the tensile strength limit of the graphite, which is ~2 times lower than its compressive strength limit.

Position of the point in the beam axis plane of a target segment	ME target		LE target	
	$< S_{eq} >$	$(S_{eq})_{max}$	$< S_{eq} >$	$(S_{eq})_{max}$
At the center (all-axis compression)	23.5	31.5	29.3	35.7
At the rounded corner (all-axis extension)	21.9	25.3	27.3	33.4

Table 3.1: The average and maximal equivalent stresses (MPa) for two target designs in case of the single turn extracted primary beam.

In case of the single turn extraction of a primary beam, the life time of targets should be determined by the maximal equivalent stress, which for given designs is 20–30% higher than the average value of stress. Taking into account results of fatigue tests for the graphite and, that the tensile strength limit of the used graphite grade is equal to 95 MPa (see previous Section), the safety factors of 2.0 and 1.6 remain for ME and LE targets respectively for the one year operation period in case of the single turn extracted primary beam.

3.2 Dynamical Stresses in the Beam Plug

The conceptual design of a beam plug, which may be used in the LE beam to decrease the high energy tail of neutrino spectrum, is given in [2]. The plug core consists of five 300 mm length and 31.7 mm diameter graphite rods (ZXF-5Q grade) encapsulated with the prestress $P_0 \simeq 5$ MPa in the 0.2 mm thick stainless steel pipe. A cooling water passes inside the water channel formed by two co-axial stainless steel pipes.

The reliability of a beam plug is determined by temperature and stresses in the most crucial situation, when the mis-steered primary proton beam directly hits the plug core (the distribution of an energy deposition density is approximately the same as in graphite targets). Results of stress calculations show, that due to an initial prestress the graphite rods remain compressed after beam heating, what provide a good thermal contact between the plug core and stainless steel pipe. The equivalent stress reaches its maximum at the proton beam axis and corresponds to the all-axis compression of a material.

Time evolution of stresses in the graphite rod with the highest energy deposition density in case of the single turn extraction of a primary beam are shown in Figure 3.7. As it follows from given plots, the maximal equivalent stress in the plug core is equal to 29 MPa what is only 5% higher than its average value. One should note, that at the regular operation mode, when the properly steered primary proton beam interacts with a production target, stresses in the plug core will be significantly smaller than in the considered here emergency situation. Taking also into account, that the compressive strength limit of the used graphite grade is equal to 210 MPa (see previous Section), one can obtain that the safety factors $\sim$4 is provided for the beam plug even in case of "the continuous emergency".

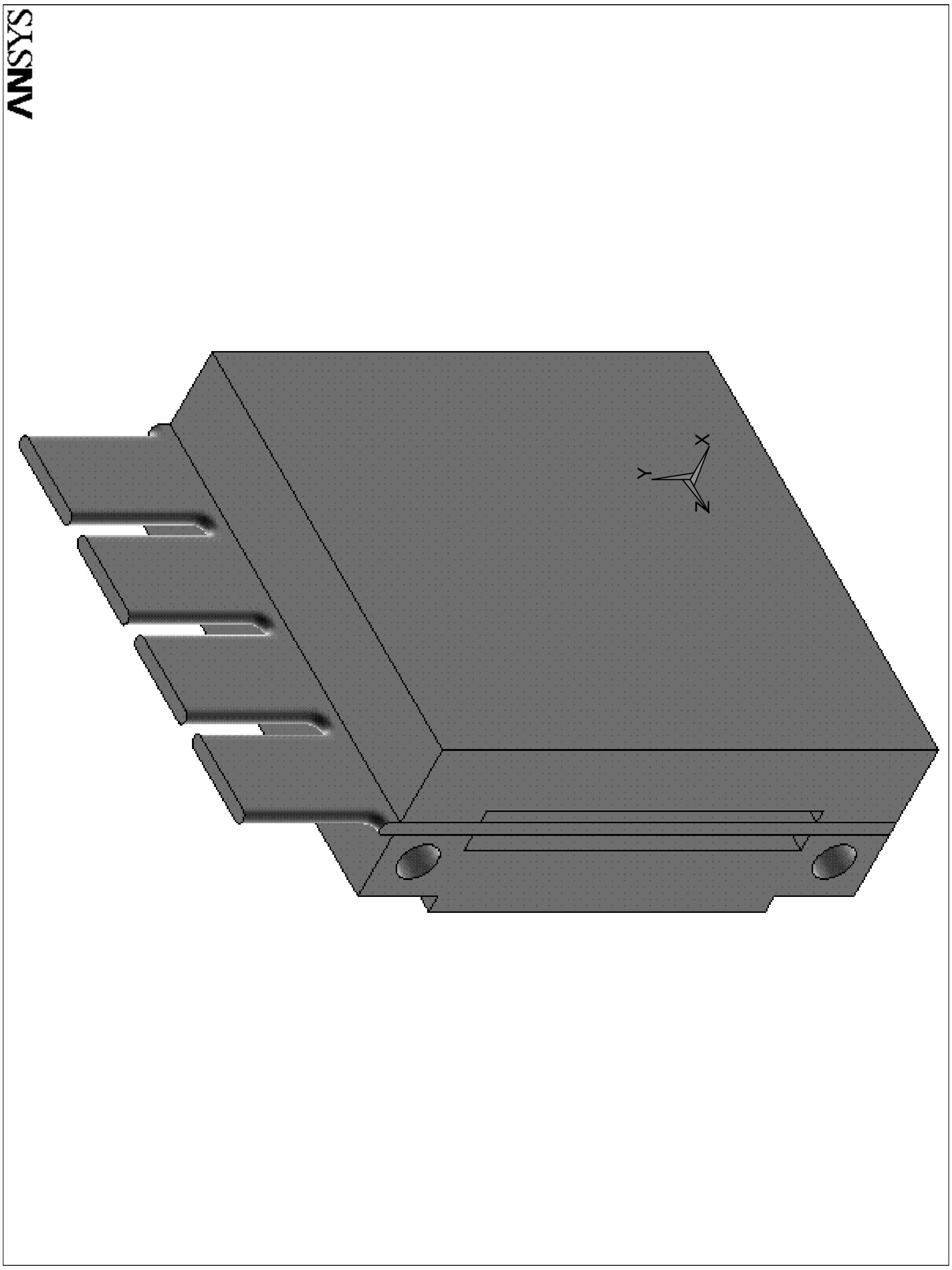

Figure 3.1: The model of a ME target for dynamic stress calculations.

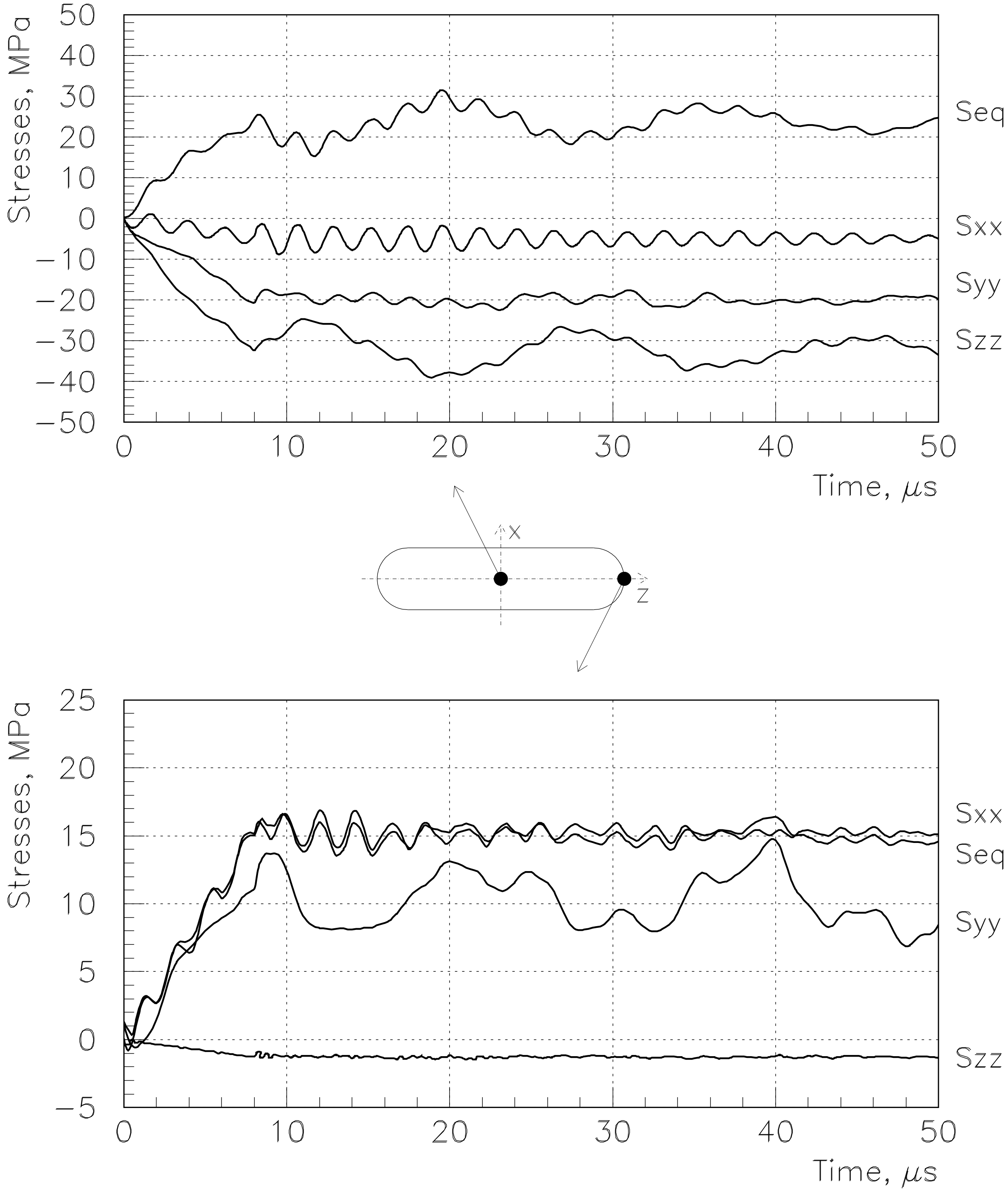

Figure 3.2: Time evolution of stresses in the ME graphite target at two points of the beam axis plane of a target segment.

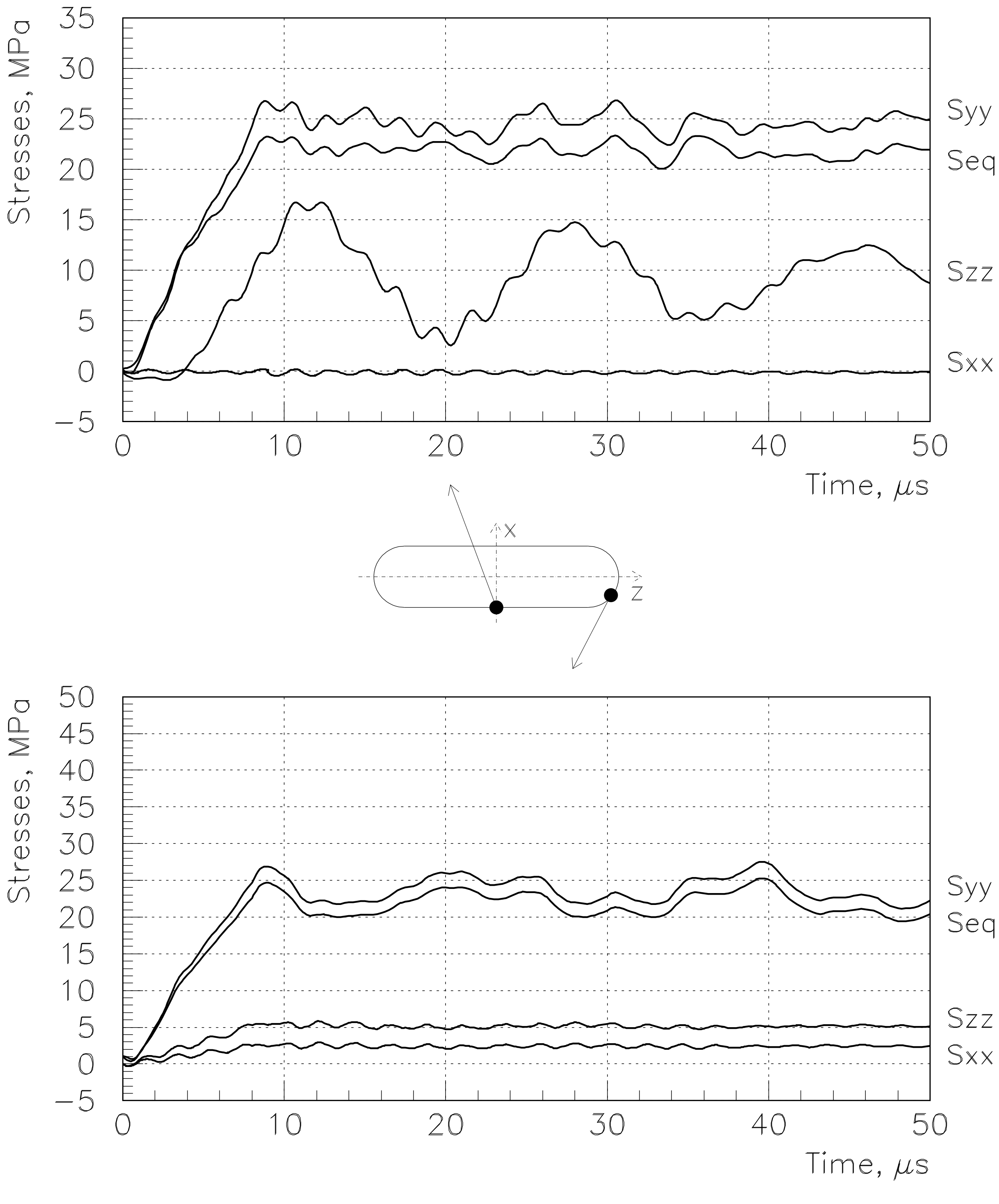

Figure 3.3: Time evolution of stresses in the ME graphite target at two points of the beam axis plane of a target segment.

Figure 3.4: The model of a LE target for dynamic stress calculations.

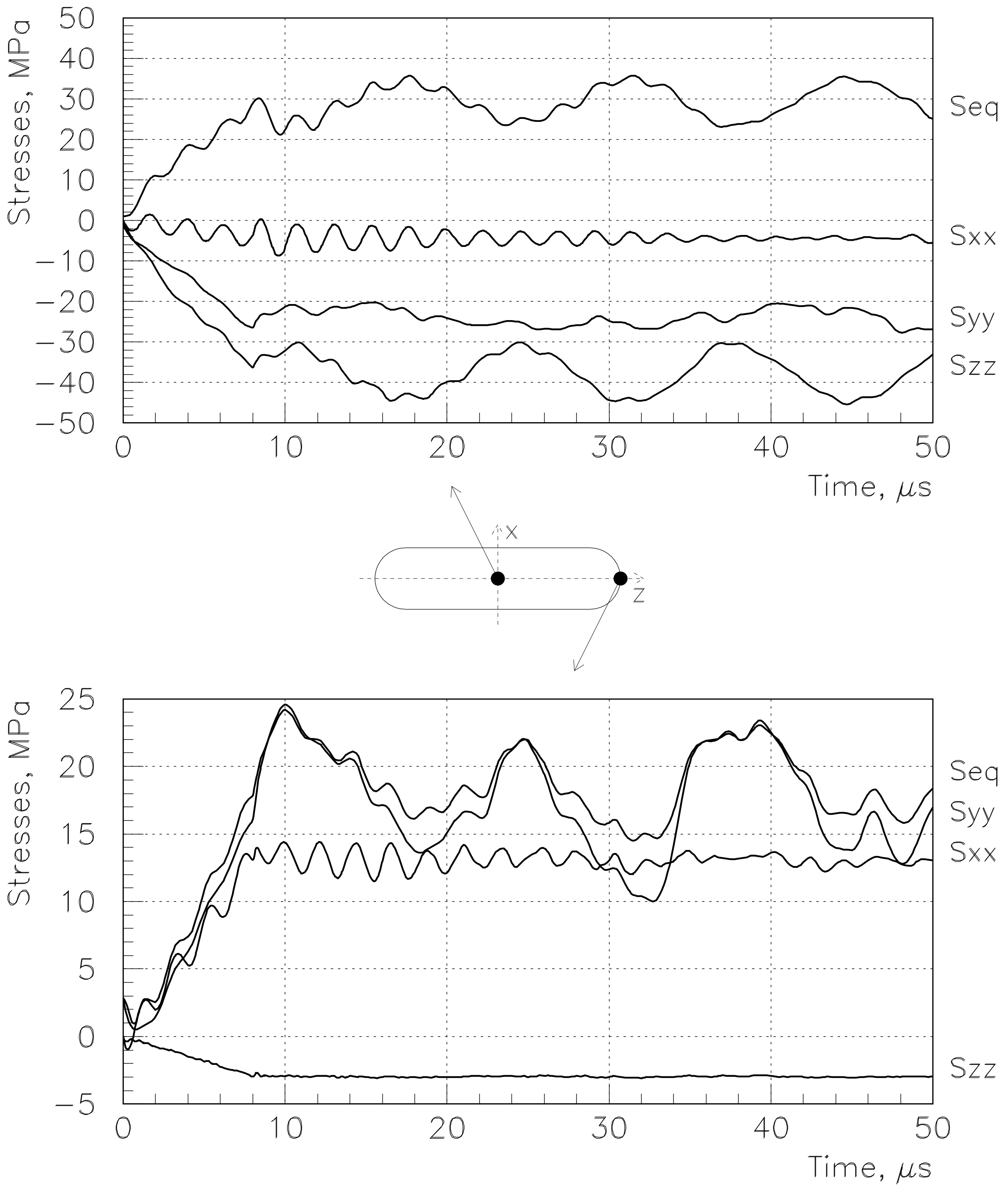

Figure 3.5: Time evolution of stresses in the LE graphite target at two points of the beam axis plane of a target segment.

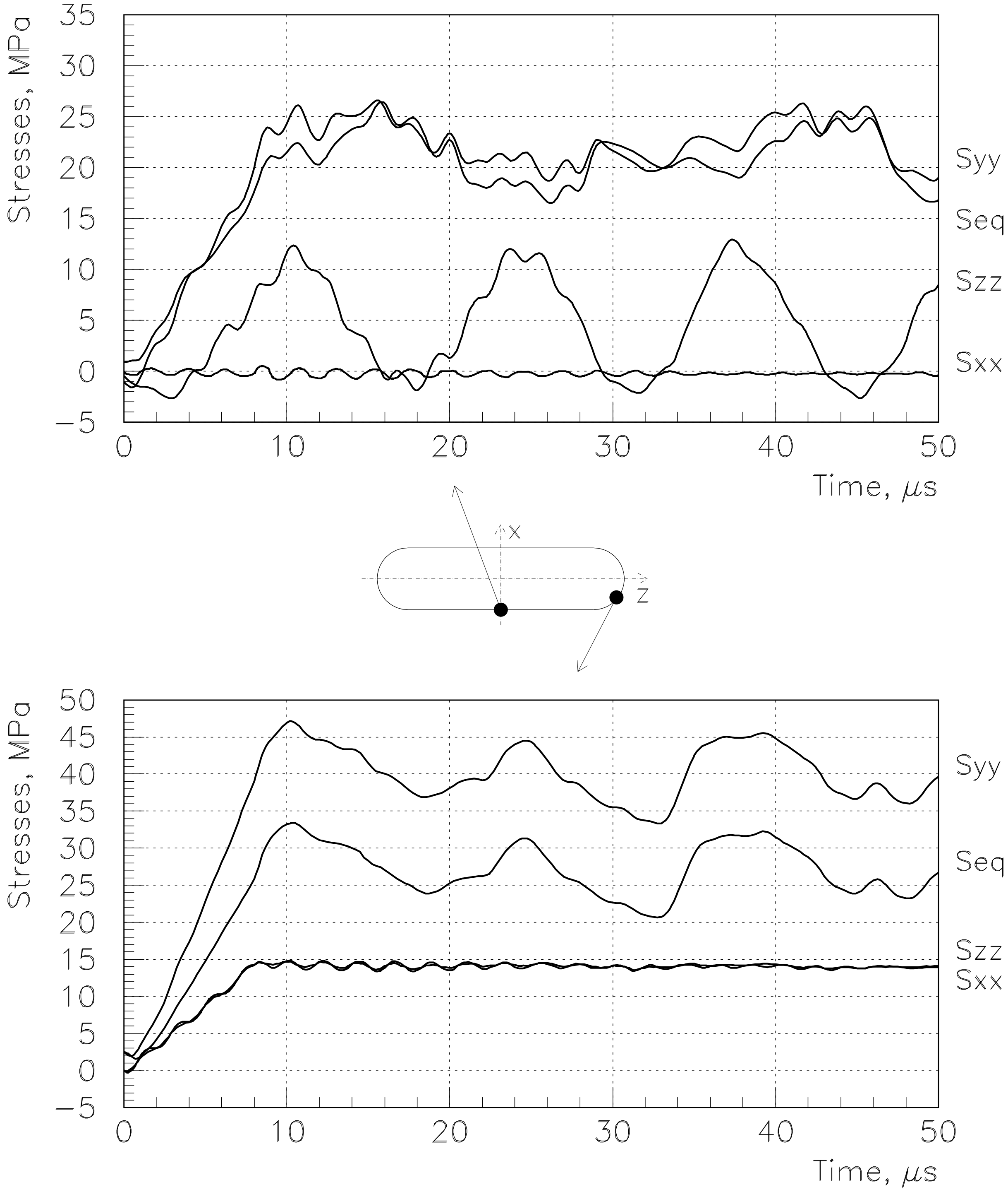

Figure 3.6: Time evolution of stresses in the LE graphite target at two points of the beam axis plane of a target segment.

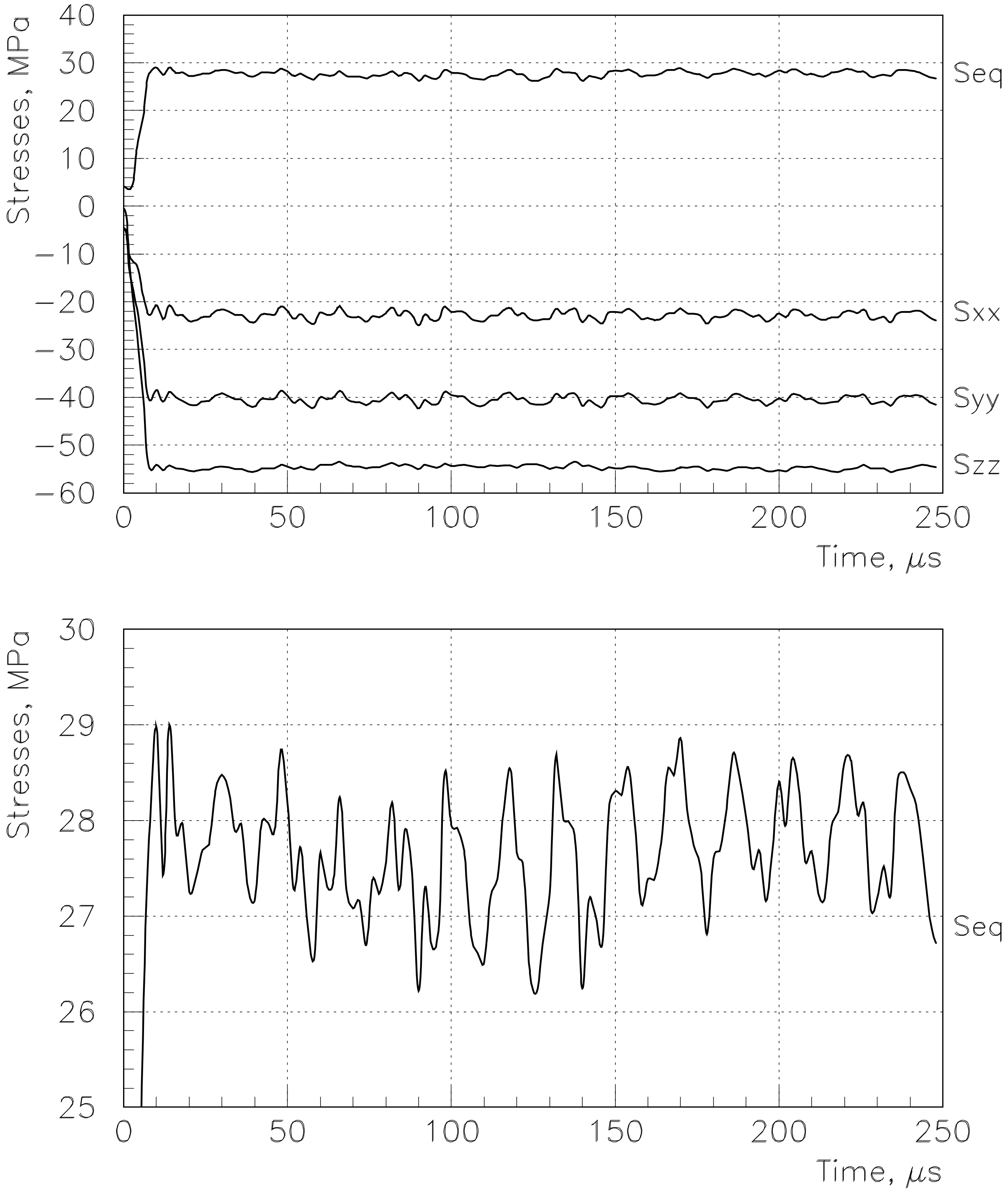

Figure 3.7: Time evolution of stresses in the beam plug core at the axis of the mis-steered primary proton beam.

4 Prototyping of the Low Energy Target

The goals of prototyping of the low energy target are to test the general construction technique and to test that alignment tolerances can be met. The main technical problem of the low energy target construction is the high reliable connection of target segments to cooling pipes. Besides this, several problems of reliable welding of different units of a target design with different sizes and properties of used materials should be solved during prototyping.

4.1 Connection of Target Segments to Cooling Pipes

4.1.1 Outline

The connection of target segments to cooling pipes should provide:

- a good thermal contact between target segments and cooling pipes;
- keeping of strength characteristics of the graphite;
- a necessary accuracy of relative positions of segments.

The possible mutual positions of cooling pipes and graphite segments are shown in Figure 4.1. The use of four pipes (variant "A") for target cooling allows to decrease approximately two times the temperature rise of a cooling water at the same water velocity, but requires essentially more complicated tooling for brazing (or soldering) than in the case of two cooling pipes (variant "B"). Because in the case of variant "B" the high straightness cooling pipes may be used as a part of tooling for brazing (or soldering) of target segments, this variant was chosen as a base one for target prototyping.

Alignment tolerances for low energy target segments were obtained from GNuMI neutrino beam simulations taking into account the factor of the neutrino event rate in the far detector (Table 4.1). Excluding a twist of target segments, providing of this accuracy of segment positioning is a quite serious problem for the $\sim$1 m length target with relatively small transverse dimensions.

The achievable accuracy of a target construction essentially depends on the temperature of brazing or soldering. It has been known that titanium hard solders with melting temperature about 1000°C are generally used for

The considered excursion of the i-th target segment ($i = 1, 2, ..., N$) from its zero position	The maximal value of excursion caused the n% decrease of neutrino event rate	
	$n = 1$	$n = 2$
The random displacement: $\Delta x_i = \Delta x_{max}(2\xi - 1), \quad \xi \in (0, 1)$	0.54 mm	0.77 mm
The sine-wave displacement: $\Delta x_i = \Delta x_{max} \sin(2\pi(i-1)/(N-1))$	0.46 mm	0.62 mm
The half sine-wave displacement: $\Delta x_i = \Delta x_{max} \sin(\pi(i-1)/(N-1))$	0.36 mm	0.51 mm
Rotation around the Z-axis (twist): $\Delta\phi_i = \Delta\phi_{max}(i-1)/(N-1)$	23 °	39 °

Table 4.1: Construction tolerances for the LE target ($N = 47$) caused the n% decrease of neutrino event rate in the far detector.

brazing of a graphite. Construction of tooling for brazing of target segments to cooling pipes at such temperature is very serious problem related with heating of an assembly to the temperature above melting point of a solder and subsequent cooling to the room temperature. The use of a soft solder allows to decrease the melting temperature up to 200–300°C and consequently essentially decrease the thermal expansion of tooling and target during the process of connection of target segments to cooling pipes.

The melting temperature of a solder defines also an allowable number of emergency spills which heat the target segment in case of the failure of a water cooling system. Such situation may occur, for example, when the water pump suddenly stops due to some reasons and the target will operate without circulating water during a few beam spills. Calculations show that in this case the target segment before each next spill will have an uniform temperature equal to an average temperature of a segment. Supposing a total absence of a water in cooling pipes, the temperature of the most heated graphite segment will reach 282°C in four beam spills.

But a water can not disappear instantaneously. Just after the first emergency spill the average temperature of a graphite segment will reach 136°C, i.e. the water in cooling pipes will boil and the average temperature of a target segment will not exceed for a time ~100°C. After the full evaporation of a water, the temperature of a target segment will reach ~300°C in four subsequent beam spills.

The time between stopping of the water pump and switching off the beam is defined by the time constant of a water rotameter used for monitoring of the water flow rate. If the time constant of a rotameter is in order of a few seconds, a soft solder with the melting temperature about 200–300°C may be used for connection of target segments to cooling pipes.

4.1.2 Prototyping of a Target Core

The 20 segments model of a target core was constructed to verify the reliability of soldering of target segments to cooling pipes and the achievable accuracy of segments location (a real target will consist of 47 segments). Target segments were cut from the 3.22 mm thick ZXF-5Q graphite plate by an electrical discharge machine. Subsequent machining of segments were made by a grinding machine.

The high difference in coefficients of a thermal expansion of the stainless steel and graphite excludes the use of stainless steel pipes. Therefore cooling pipes were rolled from the high corrosion, heat resistant and high plasticity Russian steel grade CT852 (USA analog grades: TP410, AMS5616) with the 1.6 times smaller thermal expansion coefficient. This is a martensite-ferrite class steel developed for using in hot zones of nuclear reactors. Its chemical composition, thermo-mechanical properties and the corrosion resistance are given in Tables 4.2–4.4. Temperature dependencies of thermal expansion coefficients for the CT852 steel and ZXF-5Q graphite are shown in Figure 4.2.

Element	C	Si	Mn	Cr	S	P	Ti	Cu	Ni
Composition, %	0.09–0.15	$\leq$0.8	$\leq$0.8	12–14	$\leq$0.025	$\leq$0.030	$\leq$0.2	$\leq$0.3	$\leq$0.6

Table 4.2. Chemical composition of the CT852 steel.

Ultimate strength, MPa	490
Yield strength, MPa	340
Tensile elongation, %	$\geq$20
Compressive elongation,%	60
Heat conductivity, W/m·K	31
Coeff. of thermal expansion, 10^{-6} 1/K	10.2

Table 4.3. Thermo-mechanical properties of the CT852 steel.

Environment	Depth of corrosion, mm/year
Water at 300°C	0.001
Sea water at 20°C	0.001
7%HNO_3 at 20°C	0.004

Table 4.4. Resistance to corrosion of the CT852 steel.

The process of soldering of graphite segments and cooling pipes is shown schematically in Figure 4.3:

a) soldering surfaces of graphite segments were coated with the 3–4 μm thick nickel layer by means of the magnetron spraying method and heat treated in a vacuum at the temperature of 450°C;

b) the nickel layer, as well as the steel pipe were coated with the thin layer of a soft solder with the melting temperature of ~300°C;

c) steel pipes and graphite segments were wrapped by the molybdenum wire. Four tungsten rods were used for positioning of graphite segments, while the gaps between target segments were provided by means of 0.3 mm thick spacers. This assembly was heated in vacuum to the temperature above the melting temperature of a soft solder.

Testing of samples consisting of one segment with soldered pipes show that this method of connection does not decrease the strength characteristics of the graphite. Measuring of the geometry of the 20 segment target core module shows that:

- target segments are located with respect to the longitudinal axis with the 0.11 mm standard deviation in the horizontal plane and their maximal displacement does not exceed 0.24 mm (see Figure 4.4a). This value is essentially lower than corresponding tolerances given in Table 4.1;
- maximal rotation of target segments around the vertical axis does not exceed 35 mrad (see Figure 4.4b). Using the data given in Table 4.1 for random displacements of segments in the horizontal plane, the tolerance on the rotation of segments around the vertical axis may be roughly estimated as 110 mrad for the 1% decrease of the neutrino event rate;
- maximal twist of target segments (rotation around the longitudinal axis) is negligible small (~2°) with respect to the allowable one given in Table 4.1.

4.2 Connection of Different Units of the Target Design

All welded and brazed joints were made according to the Russian standard for welding and brazing of units used in hot zones of nuclear reactors. Welded joints were made mainly by means an electron beam in a vacuum and each welded or brazed joint was tested with a helium leak detector.

4.2.1 Target Casing and Beryllium Window

To prevent an oxidation of a graphite at the high operational temperature, the target should operate in a vacuum or neutral environment, i.e. it should has vacuum tight casing. To decrease the losses of neutrino parents, target casing, in turn, should be made from a light material. The best material for casing is aluminum [2]. The use of an aluminum allows to have also the relatively small beam energy deposition in target casing, which does not require in this case of additional cooling.

Aluminum casing and availability of the stainless steel in a water cooling system lead to the necessity of a high reliable transition from the aluminum to the stainless steel. Another problem, which arises in case of aluminum casing, is connection of a beryllium window to the downstream end of a target. This problem is determined by the high difference in coefficients of the thermal expansion of an aluminum and beryllium.

1. Bimetallic transition from the aluminum to the stainless steel. This transition was constructed in two steps. The 20-30 μm thick aluminum layer was sprayed in a vacuum on the surface of the stainless steel pipe (see Figure 4.5a). After that the aluminum pipe was welded to this layer by means of an electron beam in a vacuum.

2. Welding of the metal-ceramic adapter to the stainless steel pipe. High reliable welding of the metal-ceramic adapter with the stainless steel may be achieved by the method shown schematically in Figure 4.5b. Two rings were initially welded to the adapter by means of an electron beam in a vacuum. After testing of a quality of welding with a helium leak detector, the metal-ceramic adapter was welded to the bimetallic transition and the whole assembly was welded to aluminum casing by means of an electron beam in a vacuum.

3. Beryllium window with aluminum flange and its welding to the aluminum pipe. Soldering of the beryllium to the aluminum flange is shown

schematically in Figure 4.6a. The 0.5 mm thick beryllium sheet was pressed to an aluminum ring. All contacting surfaces were preliminary coated by the 0.1 mm thick layer of the soft solder with the melting temperature equal to 300°C. Soldering was produced in a vacuum. The main problem of welding of the beryllium window to aluminum casing is the small thickness of an aluminum pipe (0.4 mm) used for target casing. Therefore welding was produced by means of an electron beam in a vacuum (see Figure 4.6b).

4.2.2 Welding of Bellows and Ceramic Adapters to Cooling Pipes

As the target is planned to be attached to the first horn, the reliability of all welded joints of water cooling pipes with bellows and ceramic adapters should be as high as possible to minimize the risk of a target failure. To obtain high reliable welding joints in a water cooling system, all welding joints were made by means of an electron beam in a vacuum. Two assemblies shown in Figure 4.7 were constructed and tested with a helium leak detector.

4.2.3 Transition from the CT852 Steel to the Stainless Steel

This problem is determined by a bad weldability of the CT852 steel with the stainless steel. The special transition from a thin pipe rolled from the CT852 steel to the stainless steel pipe was worked out during target prototyping. It is shown in Figure 4.8. The stainless steel ring was initially brazed to the CT852 steel pipe in a vacuum with the hard solder at temperature about 1150°C. After soldering of target segments to cooling pipes with preliminary brazed rings, the stainless steel pipes were welded to rings by means of laser welding.

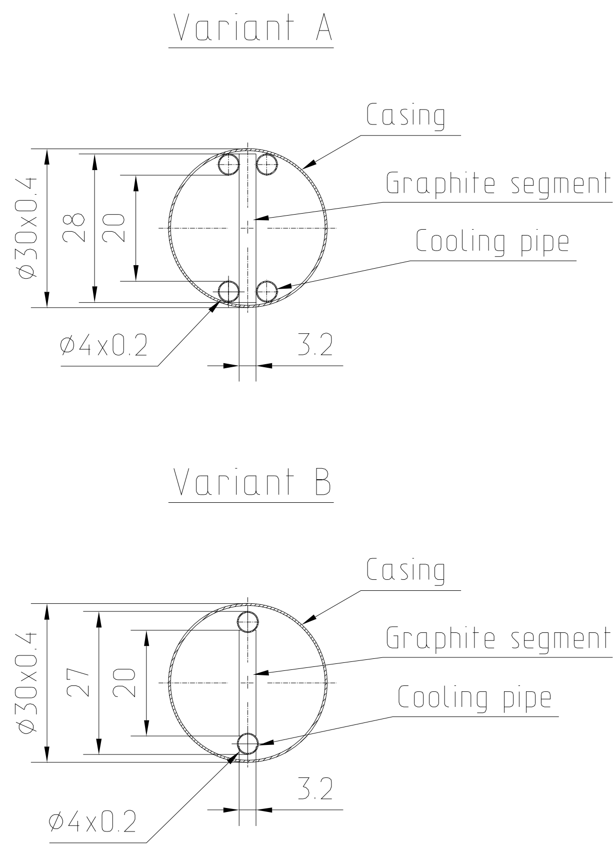

Figure 4.1: Possible positions of cooling pipes with respect to the graphite segment.

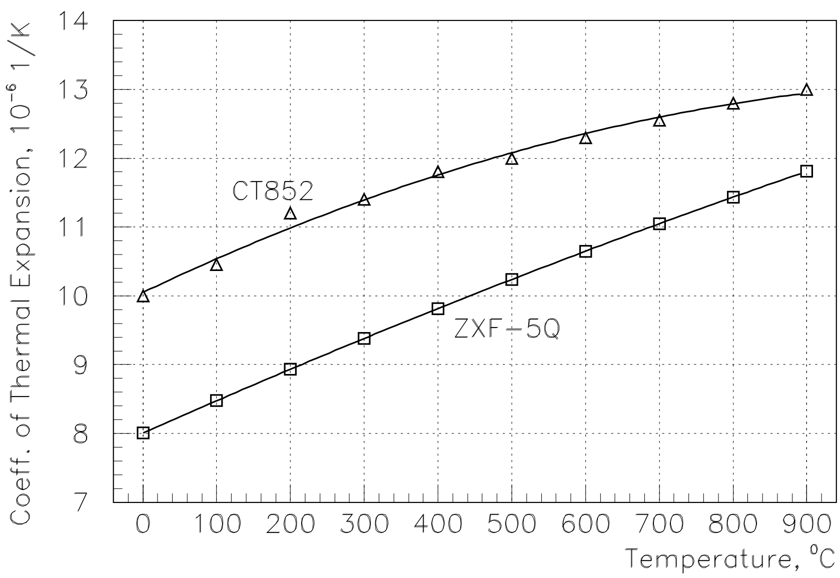

Figure 4.2: Thermal expansion coefficients vs temperature for the CT852 steel and the ZXF-5Q graphite.

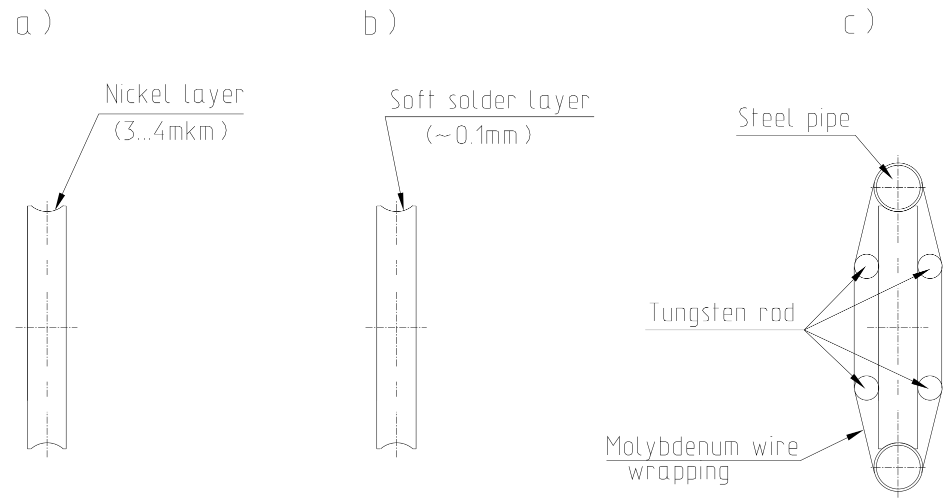

Figure 4.3: Soldering of cooling pipes to the graphite segment.

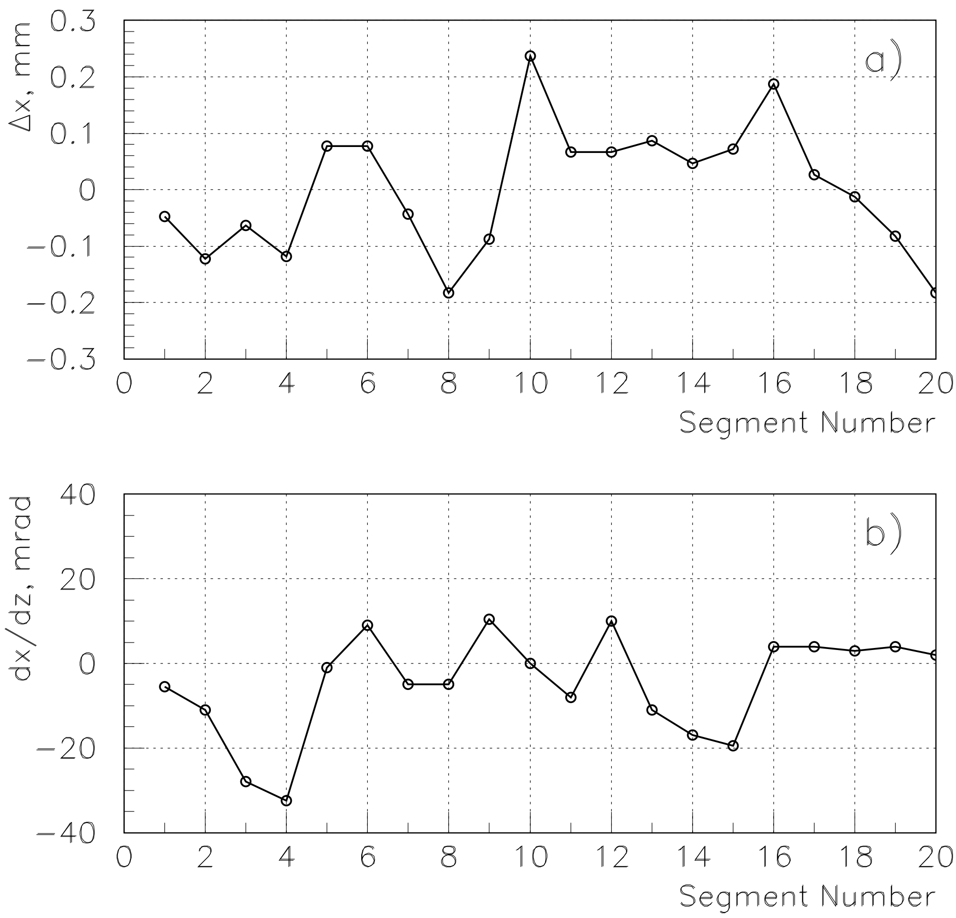

Figure 4.4: Measured linear (a) and angular (b) displacements of target segments in the horizontal plane.

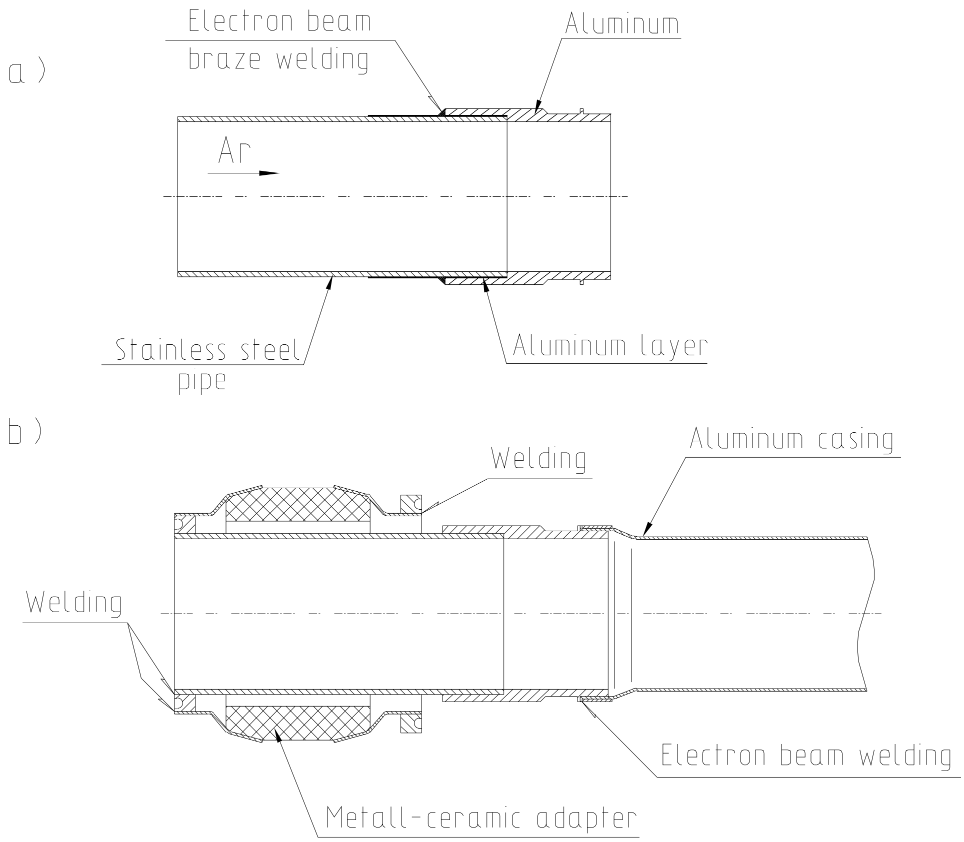

Figure 4.5: Some details of target casing: a) bimetallic transition; b) welding of the ceramic adapter and aluminum casing.

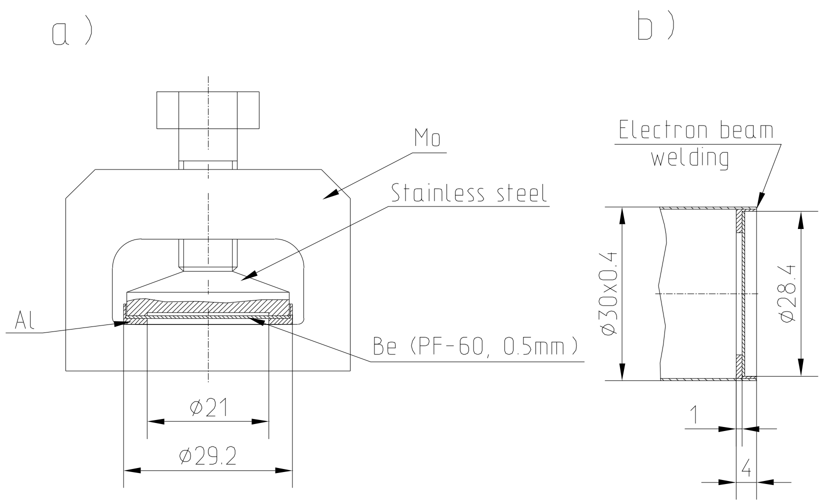

Figure 4.6: The beryllium window: a) the schematic of construction; b) welding of the beryllium window to aluminum casing.

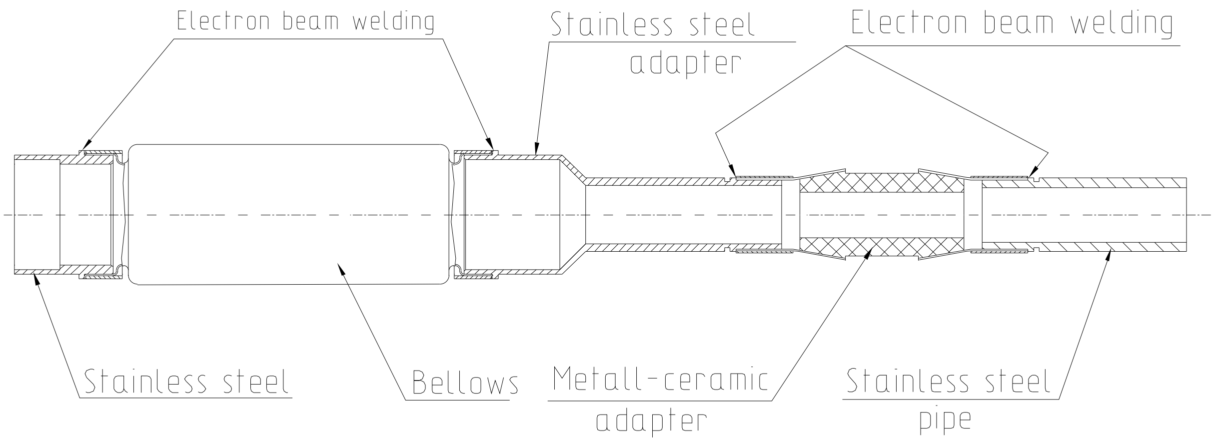

Figure 4.7: Some details of the water cooling system.

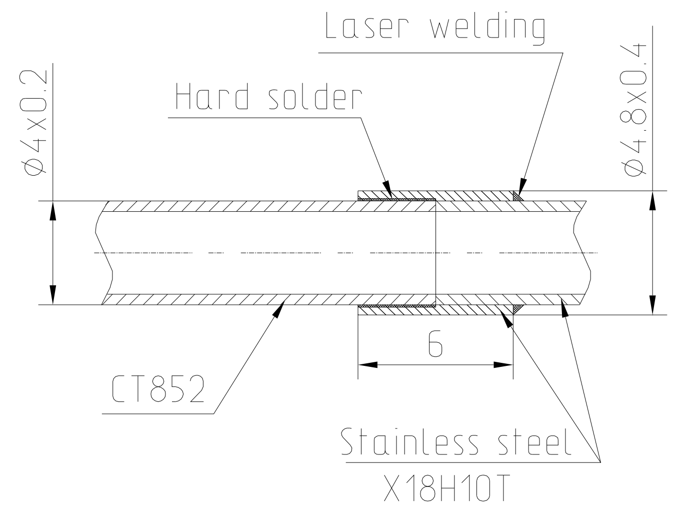

Figure 4.8: The transition from the CT852 steel to the stainless steel.

References

[1] The NuMI Facility Technical Design Report, Fermilab, 1998.

[2] Advanced Conceptual Design of the Low Energy Target and the Beam Plug, Protvino, 1999, NuMI-B-543.

[3] I.Azhgirey et al., Procedings of XV Workshop on Charged Particles Accelerators, v.2, p.270, Protvino, 1996.

[4] Brush Wellman Inc., Engineered Materials, 17876 St. Claire Avenue, Cleveland, Ohio 44110.

[5] D.E.Dombrowski, E.Deksnis, M.A.Pick, Thermomechanical properties of Beryllium, TR-1182, v.5 of the Series "Atomic and Plasma Material Interaction Data for Fusion", February 20, 1995, Int. At. En. Agency, Vienna, Austria.

[6] Poco Graphite Inc., A Unocal Company, 1601 South State Street, Decatur, Texas 76234.

[7] B.S.Wilkins, J. of Materials, 7(2), 251 (1972). B.S.Wilkins and A.K.Reich, AECL-4216 (1972).

[8] W.Kalbreier, W.Middelkoop, P.Sievers, External Targets at the SPS, CERN LAB II/BT/74-1, Geneva, 1974.

[9] The CERN Neutrino Beam to Gran Sasso (NGS), CERN 98-02, Geneva, 1998.